Optimal Power Control of Hybrid Fuel Cell Systems for an Accelerated System Warm-Up

Eric A. Müller, Anna G. Stefanopoulou, *Member, IEEE*, and Lino Guzzella, *Senior Member, IEEE*

***Abstract*—Key technical challenges in hybrid fuel cell power system applications are the power management and the thermal control. In this paper, a charge-sustaining supervisory power controller is developed, which minimizes the warm-up duration of a fuel cell/battery hybrid power system by optimally controlling the power split between the fuel cell system and the battery, as well as the operation of an auxiliary heater. The controller is implemented as a model-predictive feedback law. First, a control-oriented, mathematical model of the system is established and partially validated with experimental data. An optimal control problem is then stated, and from the necessary conditions of Pontryagin's minimum principle a solution is derived. The operation of the controller is demonstrated in the simulation, and the controller's functionality is analyzed in detail. As the controller has a feedback structure and as it requires only low computing power, it is adequate for an on-board, real-time application.**

***Index Terms*—Feedback control, fuel cell system, mathematical modeling, power management, system warm-up, time-optimal control.**

I. Introduction

FUEL CELL systems are considered to be an alternative power source for automotive propulsion, residential power systems, portable electricity generation, or back-up power supplies, due to their clean and energy-efficient mode of operation. The low operating temperature characteristics, the simple structure, and their ability to quickly respond to load changes make the polymer electrolyte membrane (PEM) fuel cells preferable for applications characterized by highly dynamic operating conditions. In most applications, a minimization of the time needed to warm up the fuel cell system is particularly important. For example, customers of fuel cell vehicles will expect to start the vehicle and drive away immediately. However, even for low-temperature fuel cell systems it is a critical task to overcome the transient power limitations during warm-up (e.g., due to water flooding in the gas diffusion layers or reduced fuel cell efficiency). A popular solution to this problem is the system hybridization. The basic idea of a hybrid setup is to combine the primary energy conversion device (the fuel cell system) with an energy storage system, such as an electrochemical battery or supercapacitors. In the case of a cold start, the energy storage system can be used to guarantee the power output demanded throughout this temperature-transient phase and, preferably in combination with an auxiliary heating device, to accelerate the system warm-up.

A system hybridization is accompanied by the question of an appropriate supervisory power management. Compared with a power system without energy storage, the hybridization creates an additional degree of freedom in the control and, thus, offers an opportunity to optimize the system performance. If the fuel cell system is equipped with an auxiliary coolant heater to enable an additionally accelerated warm-up, another degree of freedom requiring adequate control is added.

The importance of a well-designed power control strategy has been discussed in many publications, and the technical literature contains a variety of algorithms for the supervisory power management (see, for example, [1]–[6]). But all of these algorithms exclude the warm-up issues and, thus, are valid for stationary temperature conditions only. The objective is, therefore, to find an optimal power control strategy for the operation of a fuel cell/battery hybrid power system during the temperature-transient phase after a cold start. This strategy should be designed such that the fuel cells overcome the temperature-induced power limitations and efficiency losses as fast as possible and attain their operating temperature in minimum time. Simultaneously, the strategy should enable a charge-sustaining usage of the energy buffer and pay attention to the operational constraints of the fuel cells. In order to allow a real-time application of the strategy, the algorithm must not rely on a priori knowledge of the future conditions but only on the current system information. Additionally, for an on-board application the computing power required must be low.

Within the framework of this project an optimal, predictive supervisory power controller for the real-time operation of a fuel cell/battery hybrid system during the system warm-up was derived. The charge-sustaining power management developed, minimizes the warm-up duration by optimally controlling the power split between the fuel cell system and the battery, as well as, the operation of a coolant heater. The strategy is model-based and implemented as a feedback controller.

In the first part of this paper, a control-oriented, mathematical model of a fuel cell/battery hybrid power system is developed. The scope of the model is the prediction of the temperature dynamics of the fuel cell system and the estimation of the state of charge of the battery. First, an overview of the model structure is given, followed by the derivation of the model equations. The model is mainly based on the first principles and considers the relevant energy and mass flows. Fast dynamics are modeled quasi-statically and slow dynamics as constants. While the parameter values of the battery and of the power converter were assumed, the fuel cell system was calibrated and validated with experimental data.

Manuscript received February 6, 2006; revised August 31, 2006. Manuscript received in final form October 2, 2006. Recommended by Associate Editor D. E. Rivera.

E. A. Müller and L. Guzzella are with the Measurement and Control Laboratory, ETH Zurich, 8092 Zurich, Switzerland (e-mail: mueller@imrt.mavt.ethz.ch; guzzella@imrt.mavt.ethz.ch).

A. G. Stefanopoulou is with the Mechanical Engineering Department, University of Michigan, Ann Arbor, MI 48109-2121 USA (e-mail: annastef@umich.edu).

Digital Object Identifier 10.1109/TCST.2006.886435

The scope of the second part of this paper is the development of an optimal power control strategy for the operation of the hybrid fuel cell system during the warm-up period. To this end, a proper mathematical formulation of the problem is derived first. This formulation includes the definition of a reduced-order model and the statement of constraints. Applying the minimum principle of Pontryagin then results in a set of necessary conditions for the optimality of the solution. On the basis of these conditions, a feedback control law for the power management is derived. Implementation aspects for the real-time usage of the control law are then addressed, and the structure of a warm-up control system, which includes a cooling system controller, is introduced.

In the third part of this paper, the mode of operation of the control system derived is analyzed and discussed. The functionality of the control system is verified with a simulation of an optimally controlled system warm-up. A state-space illustration of the power control logic is then shown to explain the controller operation. In order to verify the controller implementation and the impact of the assumptions made during the controller development, the results of a performance benchmark are presented. Therein, a direct, open-loop optimized solution, which is based on the equations of the detailed model, is compared with the feedback controller. Finally, a comparison of the warm-up times of three alternative system configurations is given to demonstrate the benefits of a system hybridization.

II. Model of the Hybrid Fuel Cell Power System

A schematic overview of the fuel cell/battery hybrid power system considered in this project is shown in Fig. 1(a). The main elements of the configuration are a fuel cell system (including the cooling system), a power converter, and an electrochemical battery. A PEM fuel cell system installed on the test station at the University of Michigan's Fuel Cell Control Laboratory, was used to calibrate and validate the fuel cell system model.[1] Detailed information on the fuel cell stack and on the instrumentation of the test bench can be found in [7]. The electric load and the battery are connected in parallel to the main bus of the power converter. For the current application, a battery was considered that is composed of a stack of ten 7.2-V modules, with each consisting of six nickel metal hydride (NiMH) cells. Characteristic parameters of the fuel cell system, the battery, and the power converter are given in Table I.

According to the setup of the hybrid power system, the model consists of a power generation subsystem (power section, humidifier, and cooling system) and a power conversion and storage subsystem (power converter and battery). In Fig. 1(b), a causality diagram of the model is shown. The controllable inputs are the desired stack current I_{St}^{Des}, the desired air excess ratio λ_{Air}^{Des}, the coolant mass flow rate[2] $\dot{m}_{Ct}$, as well as the actuator signals of the heater u_{Ht}, and of the fan u_{Fan}. The demanded system output power P_{Out}, the ambient pressure and temperature p_{Amb} and T_{Amb}, the inlet temperature of the moist air $T_{mAir}^{HS\,In}$, and the inlet temperature of the moist hydrogen $T_{mH_2}^{PS\,In}$, are uncontrollable but measurable input signals. The main output signals of the system are the state of charge of the battery SoC, the battery current I_{Bat}, and the lumped temperatures T_{PS}, T_{HS}, and T_{CS} of the power section, the humidification section, and the cooling system, respectively. Further output signals are the local coolant temperatures at the power section outlet $T_{Ct}^{PS\,Out}$, at the humidifier outlet $T_{Ct}^{HS\,Out}$, and at the cooling system outlet (the power section inlet) $T_{Ct}^{CS\,Out}$. The model assumes high-level supervisory power control and idealized low-level control for each component. This assumption is reasonable due to a separation of time scales. It implies that $I_{St} \equiv I_{St}^{Des}$ and $\lambda_{Air} \equiv \lambda_{Air}^{Des}$.

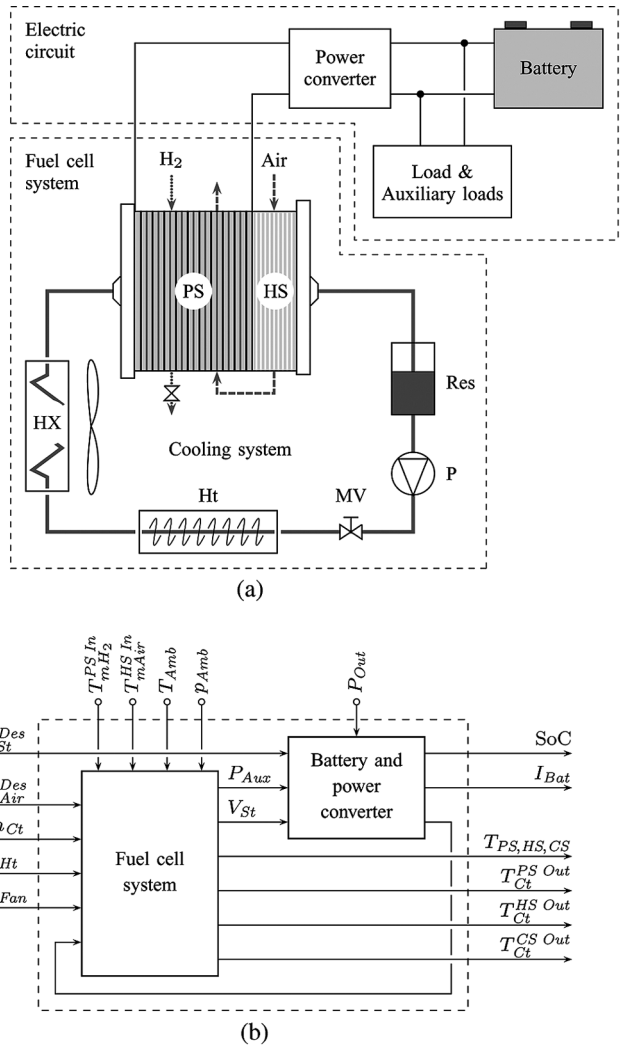

Fig. 1. Fuel cell/battery hybrid power system. (a) Schematic of the fuel cell/battery hybrid power system with fuel cell system, power converter, and battery. The fuel cell system consists of a power section (PS), an integrated humidification section (HS), and a cooling system with reservoir (Res), coolant pump (P), manual valve (MV), heater (Ht), and heat exchanger (HX). (b) Signal flow chart of the fuel cell/battery hybrid power system model.

A. Model of the Fuel Cell System

The power generation subsystem is the major element of the model. It includes the thermal dynamics of the power section, of

[1]Note that the battery and the DC/DC power converter are not part of the experimental setup.

[2]Since on the test station the flow rate of the coolant is controlled by a manual valve, rather than a coolant pump control signal, the coolant flow rate $\dot{m}_{Ct}$, is used as an input signal.

TABLE I
SPECIFICATIONS OF THE HYBRID FUEL CELL POWER SYSTEM

Characteristic	Description/value†
Type/number of fuel cells	PEM/24
Reactants	Hydrogen/air
Continuous output power (kW)	1.4
Cell active area (cm^2)	296
Membrane thickness (μm)	35
Anode gauge pressure (kPa)	14–34
Cathode gauge pressure (kPa)	<12
Preferred operating temperature range (°C)	50–65
Nominal thermal power of the heater (W)	600
.....	.....
Battery type/number of cells	NiMH/60
Nominal battery voltage (V)	72
Battery capacity @ 6.5 A (Ah)	6
Power converter efficiency	0.95

† The parameter values are manufacturer's data, were obtained by measurements, or were assumed

the humidification section, and of the cooling system, the characteristics of the gas channels, the electrochemical characteristics of the fuel cells, as well as the auxiliaries.

1) Thermal Dynamics: In order to capture the temperature dynamics of the system, the first law of thermodynamics is applied to three separate control volumes: one for the power section, one for the humidification section, and one for the cooling system. Kinetic and potential energies of the mass streams are neglected, as they are small compared with the other contributions.

For the power section, the energy balance yields the following differential equation:

$$m_{PS}C_{PS}\frac{dT_{PS}}{dt} = \dot{H}_{Reac} - P_{St} - \dot{H}_{H_2O}^{Evap\ PS} + \Delta\dot{H}_{mAir\ Exs}^{PS} + \Delta\dot{H}_{Ct}^{PS} - \dot{Q}_{Conv}^{PS2Amb} - \dot{Q}_{Rad}^{PS2Amb} - \dot{Q}_{Cond}^{PS2HS}. \quad (1)$$

The enthalpy flow rate differences of the purged hydrogen and the leaking hydrogen are not considered, as the impact of the purging and leakage on the thermal dynamics is negligibly small [7]. In the following, the relevant contributions to the energy balance (1) are detailed.

The combination of hydrogen and oxygen to form liquid product water is an exothermic chemical reaction. The energy flow rate of this reaction is calculated as the difference between the enthalpy flow rates of formation of the reactants (hydrogen and oxygen) and the enthalpy flow rate of formation of the product (liquid water) at the inlet and outlet, respectively

$$\dot{H}_{Reac} = \dot{m}_{H_2}^{Reac}\left(h_f^0 + \Delta h\right)_{H_2} + \dot{m}_{O_2}^{Reac}\left(h_f^0 + \Delta h\right)_{O_2} - \dot{m}_{H_2O}^{Reac}\left(h_f^0 + \Delta h\right)_{H_2O(l)} \quad (2)$$

where h_f^0 denotes the mass-specific enthalpies of formation with respect to a reference state. The enthalpy differences from the present state to the reference state depend upon the temperatures of the reactants and the product. The second term on the right side of (1) stands for the electric output power. The electric power delivered by the system equals the product of the stack voltage V_{St} and the current drawn I_{St}

$$P_{St} = V_{St}I_{St}. \quad (3)$$

By determining the rate at which water evaporates (or condenses) inside the power section $\dot{m}_{H_2O}^{Evap\ PS}$, from the temperatures, the pressures, and the relative humidities at the cathode inlet and the cathode outlet, respectively, the enthalpy flow rate due to evaporation (or condensation) can be calculated

$$\dot{H}_{H_2O}^{Evap\ PS} = \dot{m}_{H_2O}^{Evap\ PS}h_{fg\,H_2O}. \quad (4)$$

The parameter $h_{fg\ H_2O}$ denotes the specific evaporation enthalpy, which is a function of temperature. In order to determine the third term, which is the enthalpy flow rate of the moist air, excluding the reacting oxygen, the Dalton model is used. Hence, it is assumed that the enthalpy of the gas mixture can be evaluated as the sum of the enthalpies of the components

$$\Delta\dot{H}_{mAir\ Exs}^{PS} = \Delta\dot{H}_{Air}^{mAir\ Exs\ PS} + \Delta\dot{H}_{H_2O}^{mAir\ Exs\ PS}. \quad (5)$$

These follow from the respective mass flow rates and the temperature difference between cathode inlet and cathode outlet. The contribution of the coolant to the energy balance of the power section follows from the difference of the enthalpy flow rates between power section inlet (cooling system outlet) and power section outlet

$$\Delta\dot{H}_{Ct}^{PS} = \dot{m}_{Ct}C_{p\ H_2O(l)}\left(T_{Ct}^{CS\ Out} - T_{Ct}^{PS\ Out}\right). \quad (6)$$

The calculation of the coolant temperature at the power section outlet $T_{Ct}^{PS\ Out}$, is based on a quasistatic convective heat transfer model for a fully developed, laminar flow in a tube of rectangular cross section and uniform wall temperature. The expression for this temperature is given as

$$T_{Ct}^{PS\ Out} = T_{PS} - \left(T_{PS} - T_{Ct}^{PS\ In}\right)\cdot\exp\left(-\frac{\alpha_{PS2Ct}A_{PS2Ct}}{\dot{m}_{Ct}C_{p\ H_2O(l)}}\right). \quad (7)$$

The remaining terms in (1) describe the heat flows. As the temperatures of the fuel cell stack and its surroundings differ, heat is lost through the stack's surface. The heat transfer to the ambient consists of a convective and a radiative heat flow. Additionally, heat is transferred by conduction between the thermal reservoir of the power section and the thermal reservoir of the humidification section. The conductive heat transfer is assumed to be proportional to the conductivity, the contact area, and the temperature difference.

Similarly to (1), the energy balance for the humidification section yields a differential equation for the lumped humidifier temperature T_{HM}, as

$$m_{HS}C_{HS}\frac{dT_{HS}}{dt} = \Delta\dot{H}_{Ct}^{HS} - \dot{H}_{H_2O}^{Evap\ HS} + \Delta\dot{H}_{mAir}^{HS} - \dot{Q}_{Conv}^{HS2Amb} - \dot{Q}_{Rad}^{HS2Amb} + \dot{Q}_{Cond}^{PS2HS}. \quad (8)$$

Most terms are built up similarly to the corresponding terms of the power section. However, in contrast to (1), the term for the

reaction enthalpy rate and the term for the electric power output drop out.

The cooling system was lumped into one thermal mass of uniform temperature, and the variability of the total coolant mass due to evaporation and refill was neglected. Consequently, the differential equation defining the cooling system temperature dynamics is given as

$$m_{CS}C_{CS}\frac{dT_{CS}}{dt} = \Delta\dot{H}_{Ct}^{CS} + \dot{Q}_{Ht2CS} - \dot{Q}_{CS2Amb} \tag{9}$$

where T_{CS} is a lumped temperature. If the reduction of the coolant mass flow rate in the humidification section due to evaporation is neglected, the first term on the right side of (9) amounts to

$$\Delta\dot{H}_{Ct}^{CS} = \dot{m}_{Ct}C_{Ct}\left(T_{Ct}^{HS\ Out} - T_{Ct}^{CS\ Out}\right). \tag{10}$$

In view of the pipe volume, a time lag has to be considered for the temperature $T_{Ct}^{CS\ Out}$ at the cooling system outlet. To simplify matters, this time lag was approximated by a first-order delay

$$\tau_{CS}\frac{dT_{Ct}^{CS\ Out}}{dt} = T_{CS} - T_{Ct}^{CS\ Out} \tag{11}$$

with a (variable) time constant of

$$\tau_{CS} = \frac{\rho_{Ct}V_{CS}}{\dot{m}_{Ct}}. \tag{12}$$

The thermal power of the electric heater is assumed to be linearly dependent on the control signal u_{Ht}

$$\dot{Q}_{Ht2CS} = \dot{Q}_{Ht}^{Nom}u_{Ht} \qquad u_{Ht} \in [0,1]. \tag{13}$$

For the heat rejected at the heat exchanger, a convective transfer of heat is assumed

$$\dot{Q}_{CS2Amb} = A_{CS2Amb}\alpha_{CS2Amb}\left(T_{CS} - T_{Amb}\right). \tag{14}$$

In order to relate the convection characteristic of the heat exchanger to the fan control signal u_{Fan}, an affine approximation with the coefficients γ_{CS2Amb} and δ_{CS2Amb} is used

$$(A\alpha)_{CS2Amb} = \gamma_{CS2Amb} + \delta_{CS2Amb}u_{Fan} \qquad u_{Fan} \in [0,1]. \tag{15}$$

2) Gas Channels: A quasistatic, zero-dimensional model of the gas channels was implemented to provide data on the temperatures, the pressures, the relative humidities, and the mass flow rates of the gases. The mass storage effects in the channels are not considered, as the gas dynamics are much faster than the thermal dynamics of the system.[3] Water transport perpendicular to the membrane and water accumulation inside the cells (flooding) are not captured with this model either. Showing the model equations of the gas channels would exceed the scope of this paper.

3) Fuel Cell Stack Voltage: In order to predict the voltage output of the fuel cells, a quasistatic[4] electrochemical model was implemented. In several studies, different voltage models have been developed. In the present paper, the model of [9] was adopted, as it is calibrated and experimentally validated for the fuel cell stack considered in this project. This static voltage model considers the thermodynamic equilibrium potential E, the activation overvoltage ν_{Act}, and the ohmic overvoltage ν_{Ohm}

$$V_{Cell} = E - \nu_{Act} - \nu_{Ohm}. \tag{16}$$

Concentration losses are not considered. The overvoltages are expressed as a combination of physical and empirical relationships. The empirical parameters were determined in [9] using linear least square regression on fuel cell polarization data. The following dependencies on operational variables were identified:

$$E = E(T_{PS}, p_{O_2}^{Ca}, p_{H_2}^{\mathrm{An}}) \tag{17}$$

$$\nu_{Act} = \nu_{Act}(T_{PS}, p_{O_2}^{Ca}, i_{St}) \tag{18}$$

$$\nu_{Ohm} = \nu_{Ohm}(i_{St}, \lambda_m). \tag{19}$$

The variable i_{St} is the current density generated at the membrane surface area, while $p_{O_2}^{Ca}$ and $p_{H_2}^{\mathrm{An}}$ are the partial pressures of oxygen in the cathode and hydrogen in the anode, respectively. The variable λ_m denotes the membrane humidity. The stack voltage is defined as the sum of the individual cell voltages, which are assumed to be uniform

$$V_{St} = n_{Cells}V_{Cell}. \tag{20}$$

Note that due to the system configuration used in the present study (internal humidification section), the membrane was presumed to be always fully humidified. However, the extension of the gas channel model with a membrane humidity model is possible.

4) Auxiliary Components: For the operation of a fuel cell system, auxiliary power is needed. The main power consumers of the fuel cell system investigated are the coolant pump, the air compressor, and the electrical heater. Since the power consumptions of the former two are two to three orders of magnitude smaller than that of the electrical heater, they were neglected.[5] Note that the system investigated is a low-pressure system. The inclusion of a current-dependent air-compressor load is recommended when dealing with higher-pressure systems. The electric power of the resistance heater is assumed to be linearly dependent on the control signal u_{Ht}

$$P_{Aux} = \frac{\dot{Q}_{Ht}^{Nom}}{\eta_{Ht}}u_{Ht} \qquad u_{Ht} \in [0,1]. \tag{21}$$

B. Model of the Power Converter and the Battery

The power converter module determines the additional required power from the battery or the surplus power supplied to the battery, respectively, to provide the desired output power

$$P_{Bat} = P_{Out} + P_{Aux} - \eta_{PC}I_{St}^{Des}V_{St}. \tag{22}$$

[3]In [8], the time constants are estimated to be in the order of magnitude of 10^{-1} s for the gas dynamics and 10^{2} s for the stack temperature dynamics.

[4]In [8], the time constants of the electrochemistry and of the capacitive element of the electrode/membrane system are estimated to be in the order of magnitude of 10^{-9} s.

[5]According to the correlations for the calculation of auxiliary component power given in [10], the power input of the coolant pump is estimated to stay below 20 W, and the power input of the air compressor is assessed to be below 15 W. By contrast, the resistance heater nominally draws approximately 750 W of electric power.

The model also allows for negative values of P_{Out}. Negative power demands may occur during regenerative braking in a hybrid vehicle application, for example.

In the battery module, the battery current and the amount of energy stored are calculated. The level variable of the buffered energy is the state of charge SoC of the battery. The evaluation of the state of charge follows as

$$Q_{Bat}\frac{d\text{SoC}}{dt} = \begin{cases} -I_{Bat}, & \text{if } I_{Bat} \geq 0 \\ -\eta_{Bat} I_{Bat}, & \text{if } I_{Bat} < 0 \end{cases} \tag{23}$$

where the parameter Q_{Bat} denotes the battery capacity and η_{Bat} is the battery coulombic efficiency [11]. By convention, the battery current I_{Bat} is positive in the case of discharge. In order to avoid damage to the battery, the state of charge has to be held between a lower and an upper limit of the charge state. A basic physical model of the battery voltage V_{Bat} can be derived by considering an equivalent circuit of the system [12]. If the battery is represented by an ideal open-circuit voltage source $V_{OC}(\text{SoC})$ in series with an internal resistance $R_i(\text{SoC}, I_{Bat})$, the battery voltage results as

$$V_{Bat} = V_{OC}(\text{SoC}) - R_i(\text{SoC}, I_{Bat}) I_{Bat}. \tag{24}$$

The battery voltage is bounded by a lower and an upper limit. The open-circuit voltage $V_{OC}(\text{SoC})$ depends on the battery state of charge, whereas the internal resistance $R_i(\text{SoC}, I_{Bat})$ is a function of the battery state of charge and additionally distinguishes between charging and discharging. Both parameters are tabulated. The battery current is inferred from the battery power as

$$I_{Bat} = \frac{P_{Bat}}{V_{Bat}}. \tag{25}$$

Since the battery voltage is a function of the battery current, the latter can only be computed recursively from the battery power. The influence of temperature on the battery performance was not taken into consideration for this model. This omission is justifiable since, in order to maximize performance and lifetime of the battery packs, in many applications the battery temperature is held constant by active cooling [13], [14].

C. Parameter Estimation and Model Validation

As the model established is control-oriented and lumped-parameter, and as the formulation of the equations is mainly based on the first principles, the model is relatively easy to calibrate. Where necessary and feasible, parameter values were identified with measurement data recorded on the test bench. Many parameters are geometrical parameters and can, thus, be determined in a straightforward fashion. Others, such as heat transfer coefficients, were calculated based on known correlations, and some parameter values were estimated.

The power generation module was validated against experimental data. In order to be able to estimate the dynamic quality of the model, the important input signals were varied during the experiments. Fig. 2(a) shows the stack current I_{St}, the coolant mass flow rate $\dot{m}_{Ct}$, and the heater and fan control signals u_{Ht} and u_{Fan}, respectively. The predicted coolant temperatures at the cooling system outlet $T_{Ct}^{CS\ Out}$, and at the humidifier outlet $T_{Ct}^{HS\ Out}$, were compared with the corresponding measurement data to rate the quality of the model. As shown in Fig. 2(b), the prediction is very accurate. The root-mean-square deviation is 0.9 K for the coolant temperature at the cooling system outlet and 0.7 K for the coolant temperature at the humidification section outlet. The good agreement of the experimental data and the simulation, even during heavy transients, reveals that the model derived captures the main static and dynamic properties of the fuel cell system as expected.

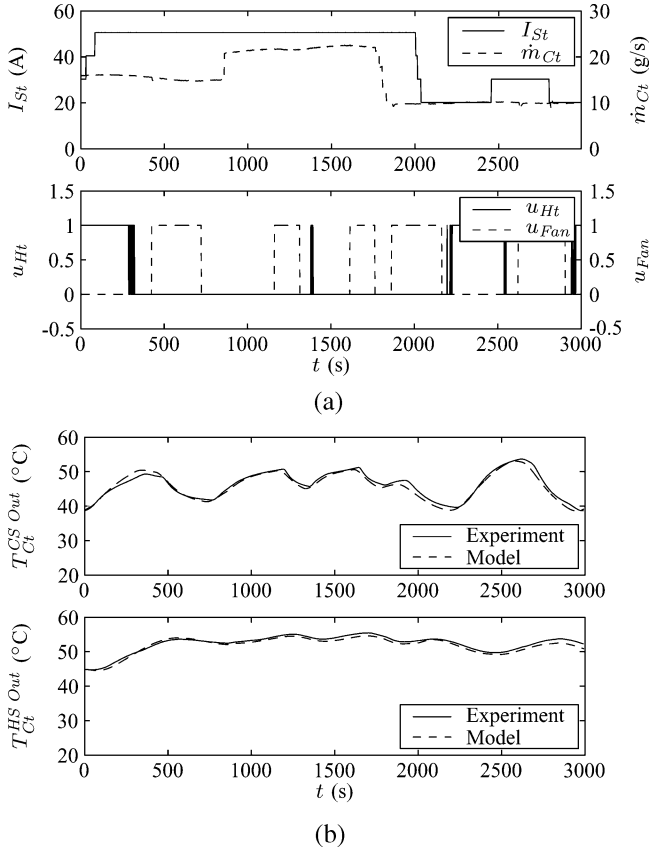

Fig. 2. Validation of the fuel cell system model. (a) Input signals (the remaining inputs of the model were assumed to be constant $\lambda_{Air}^{Des} \equiv 2$, $p_{Amb} \equiv 1.013$ bar, $T_{Amb} \equiv 25\,^{\circ}\text{C}$, $T_{mAir}^{HS\ In} \equiv 20\,^{\circ}\text{C}$, $T_{mH_2}^{PS\ In} \equiv 40\,^{\circ}\text{C}$). (b) Comparison of experiment and prediction of the coolant temperatures at the cooling system outlet (top) and at the humidifier outlet (bottom).

III. Definition of the Optimal Control Problem

The formulation of an optimal control problem requires a mathematical model of the system, the definition of constraints, and the setup of a performance functional. These elements are discussed in the following, leading to the statement of the optimal control problem.

A. System Dynamics

The fifth-order model derived in the previous section is too extensive to be used for the derivation of an optimal controller.[6] Therefore, a model of reduced complexity is proposed. This reduced-order model results from the following simplifications:

[6]However, it is applied later (Section VI) for the verification of the controller functionality, for a benchmark analysis, and to investigate various alternative system configurations.

- combination of the temperature variables T_{PS}, T_{HS}, T_{CS}, and $T_{Ct}^{PS\,Out}$ into one lumped state variable describing a mean system temperature;
- modeling the enthalpy rate of reaction $\dot{H}_{Reac}$ being independent of reactant and product temperatures;
- neglect of the enthalpy flow rate difference of the moist air across the humidification section $\Delta\dot{H}_{mAir}^{HS}$ and of the enthalpy flow rate difference of the moist excess air across the power section $\Delta\dot{H}_{mAir\ Exs}^{PS}$;[7]
- assumption that $\varphi_{mAir}^{PS\,Out} = \text{constant}$;
- removal of the heat exchanger fan input;[8]
- usage of average (constant) values for the battery open-circuit voltage and the battery internal resistance.

These simplifications yield a nonlinear, second-order system of ordinary differential equations

$$\frac{d}{dt}T_{FCS} = f_1(T_{FCS}, I_{St}^{Des}, u_{Ht}, \lambda_{Air}^{Des}, p_{Amb}, T_{Amb}) \quad (26a)$$

$$\frac{d}{dt}\text{SoC} = f_2(I_{St}^{Des}, u_{Ht}, P_{Out}, T_{FCS}, \lambda_{Air}^{Des}, p_{Amb}) \quad (26b)$$

with the state variables T_{FCS} (mean system temperature) and SoC (state of charge of the battery), and the control variables I_{St}^{Des} (desired stack current) and u_{Ht} (heater control signal). The desired air excess ratio λ_{Air}^{Des}, the output power P_{Out}, the ambient pressure p_{Amb}, and the ambient temperature T_{Amb}, are external influences (disturbances), since they are not controllable (applies for P_{Out}, p_{Amb}, and T_{Amb}) or are assumed to be controlled on a different level of the control hierarchy (applies for λ_{Air}^{Des}). Note that the coolant mass flow rate $\dot{m}_{Ct}$ does not enter the system equations of the reduced-order model. The equations of the reduced-order model are explicitly given in Appendix I and are briefly discussed in the following. Subsequently, the reduced-order model is contrasted with the detailed model to provide a verification of the simplifications previously introduced.

1) Temperature Dynamics: The differential equation of the mean system temperature T_{FCS} results from a combination of (1), (8), (9), and (11), and the consideration of the simplifications stated before. It is linear in the control variable u_{Ht} but nonlinear in the control variable I_{St}^{Des} and the state variable T_{FCS}. Additionally, it depends on the air excess ratio λ_{Air}^{Des} and the ambient pressure and temperature p_{Amb} and T_{Amb}. Please compare Appendix I for details. Most parameters of the reduced-order model follow directly from the parameters of the detailed model. Specifically, the lumped heat transfer parameters of the convective and of the radiative heat losses are calculated by summation from the heat transfer parameters of the components. However, the parameter $(mC)_{FCS}$ cannot be deduced directly from the thermal capacities of the components, as the dynamics of T_{FCS} are influenced by the time delay (11) as well. Therefore, the thermal capacity $(mC)_{FCS}$ was identified by parameter estimation.

2) Battery State of Charge: The state of charge of the battery is determined by (23) as a function of the battery current. By virtue of an approximation of the open-circuit voltage and of the internal resistance through their average values, the implicit relation for the battery current [following from (24) and (25)] can be solved. The battery power P_{Bat} follows from (22) and is a direct function of I_{St}^{Des}, u_{Ht}, and P_{Out}. Via the stack voltage, it additionally depends on T_{FCS}, λ_{Air}^{Des}, and p_{Amb}. Therefore, the differential equation for the battery state of charge is a nonlinear function of the state variable T_{FCS} and the control variable I_{St}^{Des}, and depends linearly on the control variable u_{Ht}. For details, please see Appendix I.

[7]This simplification is motivated by the results presented in [7].

[8]This represents no restriction, as the fan can be assumed to be off during the entire warm-up period for obvious reasons.

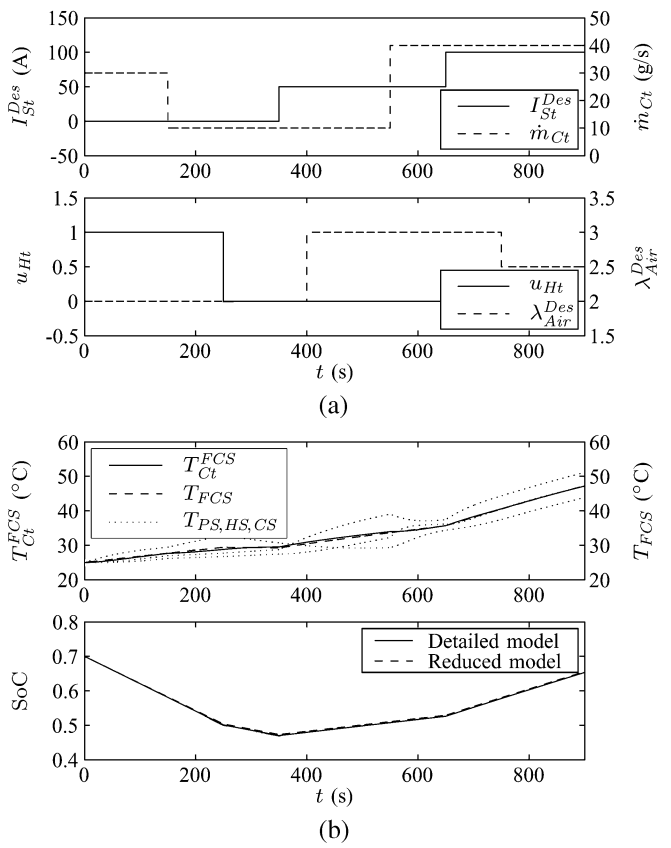

Fig. 3. Verification of the reduced-order model. (a) Input signals (the remaining inputs were assumed to be constant, $u_{Fan} \equiv 0$, $P_{Out} \equiv 500$ W, $p_{Amb} \equiv 1.013$ bar, $T_{Amb} \equiv 25\,^{\circ}$C, $T_{mAir}^{HS\,In} \equiv 20\,^{\circ}$C, $T_{mH_2}^{PS\,In} \equiv 40\,^{\circ}$C). (b) Comparison of the detailed model and the reduced-order model for the mean system temperature (top) and the state of charge (bottom).

3) Verification of the Reduced-Order Model: In Fig. 3(b), the reduced-order model is contrasted with the detailed model for a set of arbitrarily chosen, variable input signals, which are shown in Fig. 3(a). A weighted mean temperature

$$T_{Ct}^{FCS} = \frac{\sum_{j\in\{PS,HS,CS\}} m_j C_j T_{Ct}^{j\,Out}}{\sum_{j\in\{PS,HS,CS\}} m_j C_j} \quad (27)$$

was defined as a reference signal for the temperature T_{FCS}. As the results demonstrate, the reduced-order model can be applied to accurately predict the mean temperature of the system and the state of charge of the battery. This verifies that the simplifications introduced before are reasonable. Additionally, the results confirm that the coolant mass flow rate has no influence on the mean system temperature (but only on the spreading of the component temperatures).

B. Constraints

The optimal control problem formulation involves the definition of a set of admissible inputs and a requirement on the output. These elements are translated into two kinds of constraints: magnitude constraints on the control variables and terminal state constraints (i.e., constraints on the state variables at terminal time). First, the magnitude constraints are discussed, then the constraints on the terminal state are derived.

The warm-up of a fuel cell system is susceptible to being negatively affected by electrode water flooding, which reduces the effective fuel cell area. Hence, in order to optimize the warm-up phase, the accumulation of liquid water inside the cells has to be kept low. This can be achieved by limiting the stack current to a maximum value

$$I_{St}^{Des} \in [0, I_{St}^{Max}]. \tag{28}$$

As the system temperature and the reactant mass flow rates significantly affect the water removal, the stack current restriction was defined as a function of the variables T_{FCS} and λ_{Air}^{Des}

$$I_{St}^{Max} = I_{St}^{Max}(T_{FCS}, \lambda_{Air}^{Des}). \tag{29}$$

To simplify matters, the relation (28) is modified by introducing a normalized variable for the stack current control signal

$$u_{St} = \frac{1}{I_{St}^{Max}(T_{FCS}, \lambda_{Air}^{Des})} I_{St}^{Des} \tag{30}$$

to

$$u_{St} \in [0, 1]. \tag{31}$$

According to the control variable's definition (13), the magnitude constraint on the heater control signal is given as

$$u_{Ht} \in [0, 1]. \tag{32}$$

From the question of "where do we want our system to go" it is possible to derive the constraints on the state variables at terminal time. The aim was formulated that the power management strategy should be charge-sustaining over the warm-up period. A charge-sustaining operation of the hybrid power system can be guaranteed by enforcing the value of the battery's state of charge at terminal time $\mathrm{SoC}(t_f)$ to be equal or more than the initial state of charge. However, this constraint would not prevent high state of charge values, which are usually not desired (consider, for example, a hybrid vehicle application where the battery should allow to store regenerative braking energy). Therefore, an equality constraint $\mathrm{SoC}(t_f) = \mathrm{SoC}^f$ was applied to predefine the value of the battery's state of charge at terminal time. The terminal time t_f is unspecified and follows from the evolution of the temperature trajectory: when the mean system temperature T_{FCS} reaches a predefined operating temperature value T_{FCS}^f the warm-up phase is defined to be terminated. Recapitulating, the terminal state constraints are

$$T_{FCS}(t_f) = T_{FCS}^f \tag{33a}$$

$$\mathrm{SoC}(t_f) = \mathrm{SoC}^f \tag{33b}$$

where the terminal time t_f is free.

The minimum/maximum SoC and voltage constraints induced by the battery are assumed not to be violated during the warm-up phase and, thus, are not considered explicitly for the optimization. Of course, the validity of this assumption has to be verified a posteriori.

C. Performance Index

The definition of the performance index follows from the question of "how to reach the terminal state." The nominal system temperature should be attained as fast as possible in order to overcome the temperature-induced limitation of performance quickly. Accordingly, the performance index to be minimized was defined as the duration of the warm-up

$$J(u_{St}, u_{Ht}) = \int_{t_0}^{t_f} 1 dt \qquad t_f \text{ free.} \tag{34}$$

D. Optimal Control Problem

Prior to the statement of the optimal control problem, the following substitutions are introduced for the state vector, the control vector, and the vector of disturbances, in order to abbreviate the notation during the subsequent part:

$$x(t) = [x_1(t), x_2(t)]^{\mathrm{T}} = [T_{FCS}(t), \mathrm{SoC}(t)]^{\mathrm{T}} \tag{35a}$$

$$u(t) = [u_1(t), u_2(t)]^{\mathrm{T}} = [u_{St}(t), u_{Ht}(t)]^{\mathrm{T}} \tag{35b}$$

$$\begin{aligned} v(t) &= [v_1(t), v_2(t), v_3(t), v_4(t)]^{\mathrm{T}} \\ &= [\lambda_{Air}^{Des}(t), P_{Out}(t), p_{Amb}(t), T_{Amb}(t)]^{\mathrm{T}}. \end{aligned} \tag{35c}$$

The components of the signal $v(t)$ are generally not known in advance. For the formulation of the optimal control problem they are assumed to be constant

$$v(t) = v = \text{constant}. \tag{36}$$

Later, the disturbances are considered as additional controller inputs. The assumption (36) is reasonable due to the fact that rather than the fluctuations, mainly the average values of the external influences are relevant for the optimal control problem.[9]

The optimal control problem, thus, may be stated as follows.

OCP 1: Given the system

$$\dot{x}(t) = f(x_1(t), u(t), v) \quad x(t) \in \mathbb{R}^2,\ u(t) \in \mathbb{R}^2,\ v \in \mathbb{R}^q \tag{37a}$$

where v is a constant parameter vector. Let x^0 be a given initial state of the system and x^f be a specified terminal state. Find an admissible control vector $u(t) : [t_0, t_f] \to \Omega \subset \mathbb{R}^2$ with

$$u_j(t) \in [0, 1] \qquad j = 1, 2 \quad \forall t \in [t_0, t_f] \tag{37b}$$

such that the following conditions are met:

$$x(t_0) = x^0 \tag{37c}$$

$$\dot{x}(t) = f(x_1(t), u(t), v) \qquad \forall t \in [t_0, t_f] \tag{37d}$$

$$x(t_f) = x^f \tag{37e}$$

[9]Consider that the impact on the battery state of charge and on the engine temperature of the disturbances is damped by the battery capacity and by the thermal mass of the system, respectively.

and the performance index

$$J(u) = \int_{t_0}^{t_f} 1dt = t_f - t_0 \qquad t_f \text{ free} \tag{37f}$$

is minimized.

The present problem constitutes a time-invariant, minimum-time optimal control problem with a predefined terminal state at an unspecified terminal time and with magnitude constraints on the control variables. In (37d) the function $f = [f_1, f_2]^{\mathrm{T}}$ represents the system dynamics from (26a) and (26b). The condition (37e) constrains the components of the state vector at terminal time to the prescribed target state $x^f = [T_{FCS}^f, \mathrm{SoC}^f]^{\mathrm{T}}$. The Hamiltonian function $H : \mathbb{R} \times \Omega \times \mathbb{R}^2 \times \mathbb{R} \times \mathbb{R}^q \to \mathbb{R}$ associated with this optimal control problem is given by

$$H(x_1(t), u(t), \lambda(t), \lambda_0, v) = \lambda_0 + \lambda^{\mathrm{T}}(t) f(x_1(t), u(t), v) \tag{38}$$

where $\lambda(t) = [\lambda_1(t), \lambda_2(t)]^{\mathrm{T}}$ denotes the costate vector and λ_0 is a constant introduced to handle pathological cases.

IV. Solution of the Optimal Control Problem

For the solution of the optimal control problem OCP 1, the following is assumed:

- an optimal solution exists;
- the optimal control problem is not pathological (thus, we set $\lambda_0^* = 1$);
- the optimal control problem is normal (hence, that the optimal solution contains no singular arc).

Some remarks on the existence of an optimal solution and on singular solutions follow (Section IV-C).

A. Necessary Conditions for the Optimality of a Solution

The application of the minimum principle yields the following statement of necessary conditions [15], [16].

Necessary Conditions 1: If $u^*(t) : [t_0, t_f^*] \to \Omega$ is an optimal control (for the optimal control problem OCP 1), the following necessary conditions hold:

$$\dot{x}^*(t) = \nabla_\lambda H(x_1^*(t), u^*(t), \lambda^*(t), v) \tag{39a}$$
$$x^*(t_0) = x^0 \tag{39b}$$
$$x^*(t_f^*) = x^f \tag{39c}$$
$$\dot{\lambda}^*(t) = -\nabla_x H(x_1^*(t), u^*(t), \lambda^*(t), v) \tag{39d}$$

$$H(x_1^*(t), u^*(t), \lambda^*(t), v) \le H(x_1^*(t), u, \lambda^*(t), v) \quad \forall u \in \Omega, t \in [t_0, t_f^*] \tag{39e}$$
$$H(x_1^*(t), u^*(t), \lambda^*(t), v) = 0 \quad \forall t \in [t_0, t_f^*]. \tag{39f}$$

The pathological case, where $\lambda_0^* = 0$, was excluded by assumption.

In the following, the explicit statement of the time dependency is omitted for the sake of brevity.

B. Derivation of a Feedback Control Law

Next, the derivation of a feedback control law is presented. This derivation consists of two consecutive parts. As a first step, the H-minimal control is derived from the condition (39e) for the Hamiltonian function affinely approximated in the control.[10] This preliminary control law relates the control signal u to the state x and to the costate λ. In a second step, two equations are deduced from the necessary conditions (39a)–(d) and (f) in order to eliminate the costate vector.

1) H-Minimal Control: The Hamiltonian function is affinely approximated to avoid the need for any second-order condition during the minimization. Physically interpreted, this step corresponds to affine approximations of the equation for the stack power $P_{St} = P_{St}(I_{St}^{Des})$ and of the equation for the battery current $I_{Bat} = I_{Bat}(P_{Bat})$, where the coulombic efficiency of the battery is neglected. [Compare (38) and the equations of the reduced-order model given in Appendix I.] The affine approximation of the Hamiltonian in the control vector u, yields

$$\begin{aligned} H(x_1, u, \lambda, v) \approx{}& 1 + \lambda_1 A(x_1, v) + \lambda_2 C(x_1, v) \\ &+ \big[\lambda_1 B_1(x_1, v) + \lambda_2 D_1(x_1, v)\big] u_1 \\ &+ \big[\lambda_1 B_2 + \lambda_2 D_2\big] u_2 \end{aligned} \tag{40}$$

where $A(x_1, v)$, $B_1(x_1, v)$, etc. are aggregated system coefficients. If (40) is inserted into the condition (39e) for the global minimization of the Hamiltonian, and if equal terms on both sides are cancelled, the (approximative) H-minimal control can be expressed as

$$u_j^* = \begin{cases} 1, & \text{if } h_j(x_1^*, \lambda^*, v) < 0 \\ u_j^* \in [0,1], & \text{if } h_j(x_1^*, \lambda^*, v) = 0 \\ 0, & \text{if } h_j(x_1^*, \lambda^*, v) > 0 \end{cases} \qquad \text{for } j = 1, 2. \tag{41a}$$

In (41a), the following substitutions for the coefficients of the control components were introduced (switching functions):

$$h_1(x_1^*, \lambda^*, v) = \lambda_1^* B_1(x_1^*, v) + \lambda_2^* D_1(x_1^*, v) \tag{41b}$$
$$h_2(x_1^*, \lambda^*, v) = \lambda_1^* B_2 + \lambda_2^* D_2. \tag{41c}$$

Since the optimal control problem was assumed to be normal, by definition, the switching functions can be zero only at isolated instants of time [15]. Hence, the time-optimal controls u_1^* and u_2^* consist of piecewise constant functions (of value 0 or 1) with simple jumps, i.e., they are bang-bang.

2) Elimination of the Costate Vector: Under the restriction

$$0 \neq A(x_1^*, v) + B_1(x_1^*, v) u_1^* + B_2 u_2^* \approx \dot{x}_1^* \quad \forall t \in [t_0, t_f^*] \tag{42}$$

the necessary condition (39f) can be transformed into an equation for the costate component λ_1^*. If the affine Hamiltonian (40) is considered, this equation follows as

$$\lambda_1^* = -\frac{1 + \lambda_2^* \big[C(x_1^*, v) + D_1(x_1^*, v) u_1^* + D_2 u_2^*\big]}{A(x_1^*, v) + B_1(x_1^*, v) u_1^* + B_2 u_2^*} \quad \forall t \in [t_0, t_f^*]. \tag{43}$$

[10] The affine approximation of the Hamiltonian entails a suboptimality of the solution.

The substitution of (43) into the switching functions (41b) and (41c) eliminates the first costate component and, after being expanded with the denominator of λ_1^*, yields the following modified control law:

$$u_j^* = \begin{cases} 1, & \text{if } \tilde{h}_j(x_1^*, \lambda_2^*, u^*, v) < 0 \\ u_j^* \in [0,1], & \text{if } \tilde{h}_j(x_1^*, \lambda_2^*, u^*, v) = 0 \\ 0, & \text{if } \tilde{h}_j(x_1^*, \lambda_2^*, u^*, v) > 0 \end{cases} \quad \text{for } j = 1, 2 \tag{44a}$$

with the modified switching functions

$$\tilde{h}_1(x_1^*, \lambda_2^*, u_2^*, v) = \beta(x_1^*, \lambda_2^*, v) + \delta(x_1^*, \lambda_2^*, v) u_2^* \tag{44b}$$

$$\tilde{h}_2(x_1^*, \lambda_2^*, u_1^*, v) = \gamma(x_1^*, \lambda_2^*, v) - \delta(x_1^*, \lambda_2^*, v) u_1^*. \tag{44c}$$

In (44b) and (c), the existing coefficients $A(x_1^*, v)$, $B_1(x_1^*, v)$, etc. were aggregated into the new coefficients $\beta(x_1^*, \lambda_2^*, v)$, $\gamma(x_1^*, \lambda_2^*, v)$, and $\delta(x_1^*, \lambda_2^*, v)$, to shorten the notation. Further, it is presumed that

$$0 < A(x_1^*, v) + B_1(x_1^*, v) u_1^* + B_2 u_2^* \approx \dot{x}_1^* \quad \forall t \in [t_0, t_f^*] \tag{45}$$

to prevent any sign changes in the conditions of the control law (44a). This restriction is necessary due to the previous expansion with the denominator of λ_1^*. The implicit relations $u_1^* = u_1(x_1^*, \lambda_2^*, u_2^*, v)$ and $u_2^* = u_2(x_1^*, \lambda_2^*, u_1^*, v)$ following from (44a)–(c) can uniquely be solved to determine u_1^* and u_2^*, as can be shown. Details may be found in Appendix II. Consequently, the control law can be expressed as

$$u^* = u^*(x_1^*, \lambda_2^*, v). \tag{46}$$

From the necessary condition (39d) it is deduced that the costate λ_2 has to be constant on an optimal trajectory, as x_2 does not emerge in the Hamiltonian

$$\dot{\lambda}_2^* = 0 \Rightarrow \lambda_2^* = \text{constant}. \tag{47}$$

By integrating the system dynamics (39a) and considering the boundary constraints (39b) and (c), the following necessary conditions for the optimal trajectories are obtained:

$$\int_{t_0}^{t_f^*} f_1(x_1^*, u^*, v) dt = x_1^f - x_1^0 \tag{48a}$$

$$\int_{t_0}^{t_f^*} f_2(x_1^*, u^*, v) dt = x_2^f - x_2^0. \tag{48b}$$

Note that the second component of the state (which corresponds to the state of charge of the battery) does not appear in f_1 nor in f_2. The conditions (48a) and (b) can, therefore, be transformed to

$$\int_{x_1^0}^{x_1^f} \frac{f_2(x_1, u^*(x_1, \lambda_2^*, v), v)}{f_1(x_1, u^*(x_1, \lambda_2^*, v), v)} dx_1 + x_2^0 - x_2^f = 0 \tag{49}$$

by substituting

$$dt = \frac{dx_1}{f_1(x_1, u, v)} \tag{50}$$

into (48b), adapting the integration limits, and replacing u^* with the control law (46). The substitution (50) holds for $f_1(x_1, u, v) \neq 0$. The integral equation (49) is the desired relation required to remove the second costate component from the control law (46). It implicitly defines the optimal (constant) value of the second costate component

$$\lambda_2^* = \lambda_2^*(x_1^0, x_2^0, x_1^f, x_2^f, v). \tag{51}$$

Substituting (51) into (46) eventually yields the feedback control law

$$u^* = u^*(x_1, x_1^0, x_2^0, x_1^f, x_2^f, v). \tag{52}$$

The implicit equation (49) for λ_2^* guarantees that the terminal state constraints are met. It is important to note that (49) is not based upon the affine approximation of the Hamiltonian.

C. Remarks Concerning the Existence and Uniqueness of an Optimal Control and the Existence of Singular Solutions

The existence of an optimal control for all fixed t_f (including $t_f \to \infty$) implies the existence of an optimal control when the terminal time t_f is left unspecified [15]. However, the question about the existence of optimal controls from any initial state to any target set is extremely difficult to answer in general. Similarly, the proper treatment of singular solutions is very complex. Therefore, motivated from an engineering point of view, the control law derived was extended with a heuristic control law. The heuristic control law comes into operation if no zero λ_2^* of the integral equation (49) is found under the restriction $f_1(x_1, u^*(x_1, \lambda_2^*, v), v) > 0 \; \forall \; x_1 \in [x_1^0, x_1^f]$. The possible existence of multiple extremal or optimal solutions cannot be excluded, as (49) may have multiple zeros. The heuristic extension of the control law is introduced in Section V.

V. Warm-Up Control System

While in Section IV a feedback control law for the operation of the fuel cell stack and the coolant heater was derived, this section details how this supervisory power control law is augmented to an implementable controller. Together with a cooling system controller, the supervisory power controller constitutes a warm-up control system. The warm-up controller operates the hybrid power system during the temperature-transient phase, where $T_{Ct}^{FCS} \leq T_{FCS}^f$. After completion of the warm-up, the control has to be transferred to an ordinary power management strategy (sequential control).

A. Structure of the Feedback Control System

A signal flow chart of the control system is depicted in Fig. 4 The control system optimizes the system warm-up online. The power controller computes the desired stack current I_{St}^{Des} and the heater control signal u_{Ht}. Feedback signals of this controller are the mean system temperature T_{Ct}^{FCS} and the state of charge of the battery. The mean system temperature can be obtained from measurements of the coolant temperatures, according to the definition (27), whereas the state of charge has to be inferred

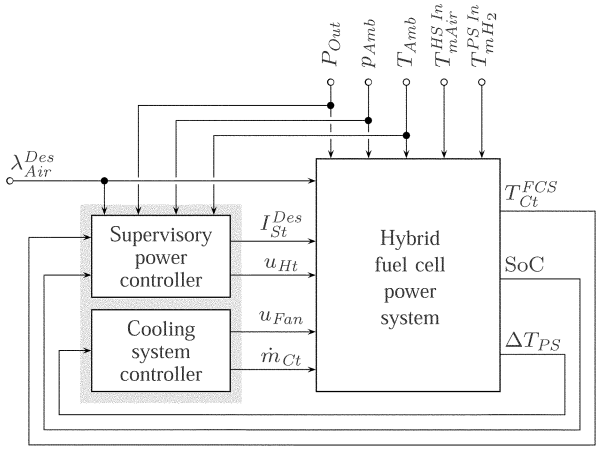

Fig. 4. Signal flow chart of the warm-up control system. The control system features a supervisory power controller and a cooling system controller.

through estimation. The details on the process of estimating the state of charge of a battery lie outside the scope of this paper and are, therefore, not considered here. For reference, see for example [17] and [18]. Aside from the feedback signals, the desired air excess ratio λ^{Des}_{Air}, the output power P_{Out}, and the ambient pressure and temperature p_{Amb} and T_{Amb}, appear as controller inputs. The desired air excess ratio is available from the air control system, whereas the disturbances P_{Out}, p_{Amb}, and T_{Amb} have to be inferred from measurements. The coolant mass flow rate $\dot{m}_{Ct}$ and the control signal of the fan u_{Fan} are regulated by the cooling system controller. The feedback signal of the cooling system controller is the difference of the coolant temperatures across the power section, $\Delta T_{PS} = T^{PS\,Out}_{Ct} - T^{PS\,In}_{Ct}$.

B. Supervisory Power Controller

The supervisory power controller is based upon the control strategy (52), which constitutes a model-predictive feedback law and operates according to the iteration scheme outlined in Fig. 5. It is assumed to work with a sample time of Δt_S and to require a computing time of Δt_C. In the following, the main parts of the control algorithm of Fig. 5 are detailed.

1) Input Signal Processing: The control law (52) determines the control signals under the assumption that the disturbance signals (35c) are constant on their average values. In practice, these signals are not known a priori. Therefore, aside from the state feedback signals, the supervisory power controller has to consider the signals λ^{Des}_{Air}, P_{Out}, p_{Amb}, and T_{Amb}, as well, in order to adapt the predicted future average values of the disturbances. Since the ambient conditions p_{Amb} and T_{Amb}, and the air excess ratio λ^{Des}_{Air}, usually do not change fast, they can be directly used as estimates for their average future values. However, the demanded output power P_{Out} can fluctuate rapidly. The prediction of the average future power demand is, therefore, inferred from the past load conditions. To this end, the power signal is low-pass filtered (with the time constant τ_{IF}) at the input of the controller.

2) Iterative Calculation of λ_2: As the equation (49) for the costate component λ_2 is an implicit equation, its solution is found iteratively. The iteration terminates if a given function tolerance (corresponding to a tolerance in the terminal state of charge) is met and aborts if a maximum number of iterations is reached, or if the constraint $f_1(x_1, u^*(x_1, \lambda_2, v_{1-4}), v_{1-4}) > 0$, is violated for any $x_1 \in [x^0_1, x^f_1]$. If the algorithm fails in finding a solution, the controller switches to the heuristic control law.

The optimal value of the costate component λ_2 would be constant for an entire warm-up if the real system behaved exactly like the model. In practice, obviously, this value has to be adapted while the warm-up proceeds. As an initial guess for λ_2, the value of the previous iteration is taken at each step.

3) Calculation of the Control Signals: If a value for λ_2 is found, the control signals are determined according to the equations of Appendix II. Alternatively, if no value for λ_2 is available, the controls are defined by heuristic rules. The reason for the choice of the heuristic rules becomes obvious later (Section VI-D), when the control law is analyzed in the state space.

1) Determine the low-pass-filtered signal of the power demand at time $\mathtt{t_j}$, where $\mathtt{t_j} = \mathtt{t_{j-1}} + \Delta\mathtt{t_S}$,

$$\mathtt{P^{IF}_{Out}(t_j)} = \mathtt{e}^{-\frac{\Delta t_S}{\tau_{IF}}}\,\mathtt{P^{IF}_{Out}(t_{j-1})} + \left(1 - \mathtt{e}^{-\frac{\Delta t_S}{\tau_{IF}}}\right)\mathtt{P_{Out}(t_j)}$$

and assign the input signals,

$$\mathtt{x^0_1} = \mathtt{T^{FCS}_{Ct}(t_j)}$$
$$\mathtt{x^0_2} = \mathtt{SoC(t_j)}$$
$$\mathtt{v_1} = \mathtt{\lambda^{Des}_{Air}(t_j)}$$
$$\mathtt{v_2} = \mathtt{P^{IF}_{Out}(t_j)}$$
$$\mathtt{v_3} = \mathtt{p_{Amb}(t_j)}$$
$$\mathtt{v_4} = \mathtt{T_{Amb}(t_j)}.$$

2) Calculate (iteratively) a constant λ_2,

$$\lambda_2 = \lambda_2(\mathtt{x^0_1}, \mathtt{x^0_2}, \mathtt{x^f_1}, \mathtt{x^f_2}, \mathtt{v_1}, \mathtt{v_2}, \mathtt{v_3}, \mathtt{v_4})$$

subject to

$$\mathtt{f_1}(\mathtt{x_1}, \mathtt{u}^*(\mathtt{x_1}, \lambda_2, \mathtt{v_{1-4}}), \mathtt{v_{1-4}}) > 0$$
$$\forall\ \mathtt{x_1} \in [\mathtt{x^0_1}, \mathtt{x^f_1}]$$

with

$$\mathtt{x^f_1} = \mathtt{T^f_{FCS}}$$
$$\mathtt{x^f_2} = \mathtt{SoC^f}.$$

3) If an admissible value for λ_2 was found, calculate the optimal control signals,

$$\mathtt{u_1} = \mathtt{u^*_1}(\mathtt{x^0_1}, \lambda_2, \mathtt{v_{1-4}})$$
$$\mathtt{u_2} = \mathtt{u^*_2}(\mathtt{x^0_1}, \lambda_2, \mathtt{v_{1-4}}).$$

Else (if no admissible value for λ_2 was found), determine heuristically motivated control signals,

$$[\mathtt{u_1}, \mathtt{u_2}]^{\mathtt{T}} = \begin{cases} [0,0]^{\mathtt{T}} & \text{if } \mathtt{x^0_2} \geq \mathtt{x^f_2} \\ [1,0]^{\mathtt{T}} & \text{if } \mathtt{x^0_2} < \mathtt{x^f_2} \end{cases}.$$

4) Assign the output signals,

$$\mathtt{I^{Des}_{St}} = \mathtt{u_1} \cdot \mathtt{I^{Max}_{St}}(\mathtt{x^0_1}, \mathtt{v_1})$$
$$\mathtt{u_{Ht}} = \mathtt{u_2}$$

for $\mathtt{t_j} + \Delta\mathtt{t_C} \leq \mathtt{t} < \mathtt{t_{j+1}} + \Delta\mathtt{t_C}$, and $\mathtt{t_{j+1}} = \mathtt{t_j} + \Delta\mathtt{t_S}$.

Fig. 5. Iteration scheme of the supervisory power controller.

C. Cooling System Controller

The cooling system controller determines the operation of the fan and the rate of coolant flowing. During the warm-up, the fan is off

$$u_{Fan} \equiv 0 \qquad \forall\, T_{Ct}^{FCS} \leq T_{FCS}^{f}. \tag{53}$$

Upon completion of the warm-up, the fan has to be operated to hold the desired system temperature. The coolant flow rate $\dot{m}_{Ct}$ is controlled such as to avoid large temperature gradients within the fuel cell stack. This guarantees a high conversion efficiency of the fuel cells on the one hand and avoids damage to the stack through mechanical stress or local temperature peaks, on the other hand. The coolant flow controller was realized as a PI controller with an artificial output saturation and an anti-reset windup addition. The artificial output saturation

$$\dot{m}_{Ct} \geq \dot{m}_{Ct}^{Min} \tag{54}$$

ensures that the controller keeps a minimum flow rate during low power conditions. During high power demands, the coolant flow rate is increased such that a maximally allowed temperature difference over the power section (the set-point of the controller) ΔT_{PS}^{Max}, is not (severely) exceeded.

D. Controller Settings and Application Parameters

The operation of the power controller is defined by the values of the target temperature T_{FCS}^{f}, the target state of charge of the battery SoC^{f}, the stack current constraint $I_{St}^{Max}(T_{FCS}, \lambda_{Air}^{Des})$, the input filter time constant τ_{IF}, and the sample time Δt_S. The cooling system controller, on the other hand, relies on the parameters of the minimum coolant mass flow rate $\dot{m}_{Ct}^{Min}$, and the maximum temperature gap across the power section ΔT_{PS}^{Max}. Aside from the controller settings, the warm-up controller also includes the parameters of the reduced-order system model.

VI. Results and Discussion

As a basis for the subsequent evaluation some preliminary definitions are required. First, nominal operating conditions and controller settings are defined. Then, a direct, open-loop optimization method is introduced. Open-loop optimized solutions were used for two purposes. For one, they served as performance benchmarks for the feedback controller. Second, the direct optimization method was applied to quantify the influence on the warm-up time of the hybridization and of the extension of the fuel cell system with an auxiliary heater.

A. Controller Settings and Nominal Operating Conditions

The nominal operating conditions and controller settings are given in Table II. Two cases are distinguished. For both cases, the desired terminal temperature of the fuel cell system (the temperature at which the warm-up is defined to be completed) is set to the lower bound of the preferred fuel cell operating temperature range, namely $T_{FCS}^{f} = 50\,^{\circ}\mathrm{C}$. A typical value of $\mathrm{SoC}^{f} = 0.7$ is used to predefine the terminal state of charge of the battery. For the maximum stack current, a variable upper limit, $I_{St}^{Max} = I_{St}^{Max}(T_{FCS}, \lambda_{Air}^{Des})$, is defined for case 1 to take into account cold-start transient power limitations. A constant value of $I_{St}^{Max} = 148$ A is specified for case 2.[11] In the present project, the variable current limit was chosen arbitrarily. However, a more sophisticated approach, for instance, based on a model of the membrane and the gas diffusion layers, could alternatively be applied.[12] The time constant of the input filter is defined as $\tau_{IF} = 60$ s. It can be shown that the choice of the time constant is not critical, i.e., over a broad range of values the elapsed warm-up time is only slightly affected by τ_{IF}. For the sample time of the power controller, a value of $\Delta t_S = 3$ s is assumed. Some comments on the choice of the sample time follow in Section VI-C. The mass flow rate of the coolant is assumed to be controlled by the cooling system controller for case 1 and is set to $\dot{m}_{Ct} = 35$ g/s for case 2. The parameter values of the cooling system controller are defined as $\Delta T_{PS}^{Max} = 10\,^{\circ}\mathrm{C}$ for the maximum temperature gap over the power section, and as $\dot{m}_{Ct}^{Min} = 10$ g/s for the minimum coolant mass flow rate, respectively. The nominal values of the input signals represent typical operating conditions of the power system. All signals are constant, except for the power demand of case 2, which is time-variant. The system is initialized as follows: the temperature variables are initialized with ambient temperature, whereas the initial condition of the battery charge is set to $\mathrm{SoC}(0) = 0.7$.

TABLE II
Definition of Controller Settings and Nominal Operating Conditions

Parameter/signal	Symbol	Value	
		Case 1	Case 2
Desired terminal temperature	T_{FCS}^{f}	50°C	
Desired terminal state of charge	SoC^{f}	0.7	
Constraint for stack current	I_{St}^{Max}	variable	148 A
Input filter time constant	τ_{IF}	60 s	
Sample time of power controller	Δt_S	3 s	
Coolant mass flow rate	$\dot{m}_{Ct}$	controlled	35 g/s
Maximum temperature gap (PS)	ΔT_{PS}^{Max}	10°C	-
Minimum coolant mass flow rate	$\dot{m}_{Ct}^{Min}$	10 g/s	-
Power demand	P_{Out}	variable	500 W
Desired air excess ratio	λ_{Air}^{Des}	2	
Ambient pressure	p_{Amb}	1.013 bar	
Ambient temperature	T_{Amb}	25°C	
Air inlet temperature	$T_{mAir}^{HS\,In}$	20°C	
Hydrogen inlet temperature	$T_{mH_2}^{PS\,In}$	40°C	
Initial temperatures (PS, HS, CS)	$T_{(\cdot)}(0)$	25°C	
Initial state of charge	$\mathrm{SoC}(0)$	0.7	

B. Direct Open-Loop Optimization

Besides the development of a feedback controller, the optimal control problem considered was also solved by a direct trajectory optimization method in an open-loop manner, based on the detailed, fifth-order model of the system. Therefore, the problem of minimizing the warm-up time was implemented in GESOP, a software system for numerical trajectory optimization of dynamic systems [21]. In order to discretize the optimal control problem and to transcribe it into a parametrized, finite-di-

[11] This value for the maximum stack current corresponds to a maximum current density of 0.5 A/cm^2.

[12] Compare, for example, [19] and [20].

mensional optimization problem, the multiple shooting method PROMIS[13] was used. The standard nonlinear program solver SLLSQP[14] was then applied to solve the resulting algebraic optimization problems for various operating conditions and parameter values. The control signals were approximated by piecewise linear functions. For the problem at hand, the number of corresponding subintervals was set to 12, resulting in 11 internal nodes whose positions, in turn, are subject to optimization. Additional control refinement points were defined where necessary.

C. Simulation of an Optimally Controlled System Warm-Up Under Variable Operating Conditions

In order to demonstrate the full functionality of the feedback control system, a simulated warm-up under variable power demands was analyzed. The simulation is based on the detailed model of the system. For this analysis, the nominal controller settings and operating values of case 1 (Table II) were used. In Fig. 6(a) the variable power demand P_{Out} and the low-pass-filtered power signal P_{Out}^{IF}, are displayed. The first and the second subplots of Fig. 6(b) show the output signals of the supervisory power controller I_{St}^{Des} and u_{Ht}, respectively. The transient power limitation of the current is indicated by a dotted line. The heater signal u_{Ht}, is selected between 0 (off) and 1 (on with nominal power). In the third subplot, the mean system temperature T_{Ct}^{FCS} and the component temperatures T_{PS}, T_{HS}, and T_{CS} are shown. The state of charge of the battery SOC is shown in the fourth graph. The terminal conditions $T_{FCS}^{f} = 50\,^{\circ}\mathrm{C}$ and $\mathrm{SoC}^{f} = 0.7$, are each identified by a triangle. In the fifth subplot the battery current I_{Bat}, is plotted. Positive values mean discharging of the battery, negative values indicate charging. The lowermost subplot of Fig. 6(b) shows the control signal $\dot{m}_{Ct}$ of the cooling system controller and the feedback signal ΔT_{PS}.

At the beginning of the warm-up, the heater is on and the power is drawn from the battery. Consequently, the temperature of the system (specifically the temperature of the cooling system) rises and the state of charge of the battery decreases. After approximately 190 s the fuel cell stack is turned on to generate the maximum allowed electric power. The surplus power recharges the battery and the waste heat of the stack causes an increased heat flow to the system. After an elapsed time of approximately 300 s, the heater is switched off. Towards the end of the warm-up, the heater is switched on again, and the controller toggles the control signals to compensate for prediction errors.[15] The warm-up is defined to be completed when the terminal temperature is reached. In the sample simulation shown in Fig. 6, a warm-up time of 438 s results (indicated by a dotted vertical line). During the entire warm-up phase, the power controller keeps the fuel cell stack within the operating limits (i.e., the stack current does not exceed the variable current constraint). At the end of the warm-up phase the predefined state of charge of the battery is met exactly, although the controller does not know the power profile a priori.

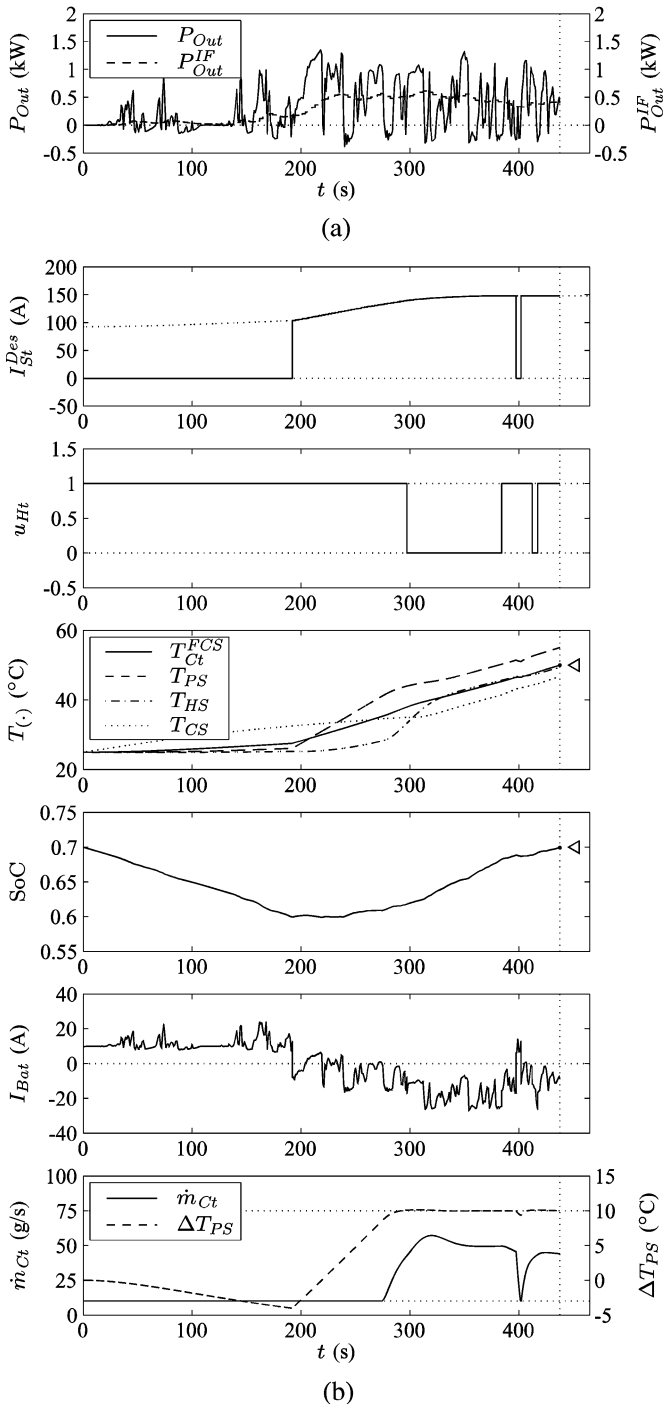

Fig. 6. Simulation results of an optimally controlled system warm-up under nominal operating conditions (case 1 of Table II). (a) Power demand and low-pass filtered power signal; (b) control signals and resulting system trajectory.

The cooling system controller regulates the coolant mass flow rate as expected. When the heat generation inside the power section is low, the coolant mass flow rate is at its minimum value (10 g/s). Once the maximum tolerated temperature difference (10 °C) is reached, the controller increases the mass flow rate accordingly, in order to maintain the conditions. During this phase, temperature overshoots of less than 0.2 °C are observed. Implemented in Matlab 6.5.1 and processed on an Intel Pentium III, 1.2-GHz Mobile CPU, the maximum computing time that is needed for the power controller to determine its next move is

[13]Parametrized trajectory optimization by direct multiple shooting.

[14]Sequential linear least squares quadratic programming.

[15]Generally, two possible sources of prediction errors arise. First, a model is always only an idealized representation of the real system. Second, the time dependent evolution of the external signals are (usually) not known in advance.

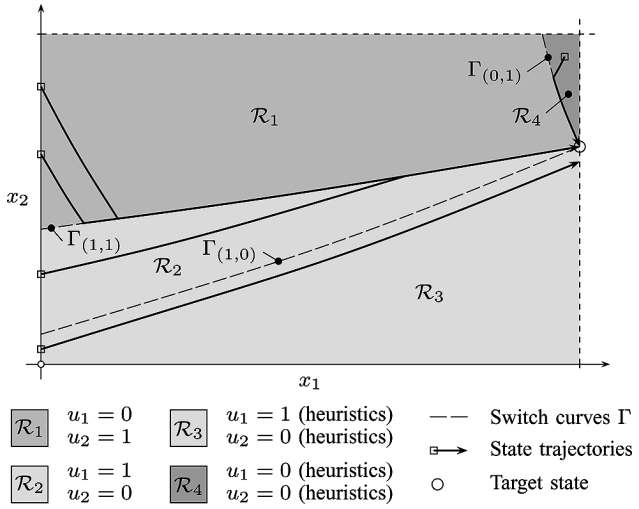

Fig. 7. State-plane illustration of the power controller.

TABLE III
BENCHMARK RESULTS FOR THE POWER CONTROLLER UNDER VARIOUS OPERATING CONDITIONS

Operating conditions	$J^{*\dagger}$ (s)	$\delta J^{\ddagger}$ (%)
Case 2 of Table II	309	0.0
Case 2 of Table II but $P_{Out} = 250\,\mathrm{W}$	362	0.1
Case 2 of Table II but $P_{Out} = 750\,\mathrm{W}$	272	2.3
Case 2 of Table II but $P_{Out} = 1200\,\mathrm{W}$	236	0.7
Case 2 of Table II but $\lambda_{Air}^{Des} = 3$	335	0.7
Case 2 of Table II but $T_{Amb} = T_{(\cdot)}(0) = 15°\mathrm{C}$	436	0.1
Case 2 of Table II but $\mathrm{SoC}(0) = 0.6$	240	0.7
Case 2 of Table II but $\mathrm{SoC}(0) = 0.8$	410	0.2
Case 2 of Table II but $\mathrm{SoC}^f = 0.6$	410	0.2
Case 2 of Table II but $\mathrm{SoC}^f = 0.8$	240	0.6

† Minimum warm-up time (direct, open-loop optimization)
‡ Relative performance loss of the controller:
$\delta J = (J|_{\mathrm{Closed-loop}} - J^*)/J^*$

1.51 s, in contrast to a sample time of $\Delta t_S = 3$ s. The average computing time amounts to 0.16 s.

D. Illustration of the Supervisory Power Controller in the State Space

In this section, the operation of the supervisory power controller is analyzed in the state space. If constant operating conditions are assumed, there are sets or regions of the state space over which the control signals are constant (0 or 1), since the control signals of the power controller are piecewise constant functions of time, but also functions of the states. In a 2-D state space, these sets are separated by switch curves. It is the equation and shape of these switch curves that determine the control actions. A schematic of the power controller's switch curves for typical conditions is sketched in Fig. 7. Note that the exact shape and position of the switch curves varies with the operating conditions (e.g., the value of P_{Out}) and the controller settings (the target state vector and the stack current constraint). The switch curve $\Gamma_{(1,1)}$ is the locus of all points (x_1, x_2) which can be forced to the target state (x_1^f, x_2^f) by the control $u = [1,1]^{\mathrm{T}}$. Similarly, the controls $u = [1,0]^{\mathrm{T}}$ and $u = [0,1]^{\mathrm{T}}$ define the switch curves $\Gamma_{(1,0)}$ and $\Gamma_{(0,1)}$, respectively. It follows from the control law that the stack control signal is zero $u_1 = 0$, and the heater is on $u_2 = 1$, for state vectors inside the region $\mathcal{R}_1$. Inside the region $\mathcal{R}_2$, the control signals are $u_1 = 1$ and $u_2 = 0$. The regions $\mathcal{R}_3$ and $\mathcal{R}_4$ represent the sets of state vectors for which the control law yields no solution. Inside these areas, the controls are determined by the heuristic rules: If $x_2 < x_2^f$, the fuel cell stack is turned-on, $u_1 = 1$, and the heater switched-off, $u_2 = 0$. However, if $x_2 \geq x_2^f$, both control signals are zero, $u_1 = u_2 = 0$. The optimal state trajectories are defined by a sequence of control actions. Every trajectory starting in $\mathcal{R}_1$ is forced to the target state by a control sequence $\{[0,1]^{\mathrm{T}}, [1,1]^{\mathrm{T}}\}$, where the control switches at the moment the trajectory reaches the $\Gamma_{(1,1)}$ switch curve. Equally, trajectories starting in the set $\mathcal{R}_2$ reach the target state by a control sequence $\{[1,0]^{\mathrm{T}}, [1,1]^{\mathrm{T}}\}$. Inside the region $\mathcal{R}_4$, the heuristic rules cause the system to reach the $\Gamma_{(0,1)}$ switch curve. The $\Gamma_{(0,1)}$ switch curve then leads the system to the target state. By contrast, when starting in $\mathcal{R}_3$, the heuristic controls force the system trajectory to proceed in parallel to the region boundary. Hence, with a bang-bang control, trajectories inside the set $\mathcal{R}_3$ cannot reach the target state. However, with the control $u = [1,0]^{\mathrm{T}}$, the system is forced to get as close as possible to the target state.

E. Benchmark Analysis for the Supervisory Power Controller

During the development of the power controller, at some points certain approximations or assumptions had to be made (e.g., model reduction, linearization of the Hamiltonian). In order to quantify their impact and that of the discrete controller operation on the performance of the controller, some performance values of the feedback controller, applied to the detailed model, were compared with the optimal warm-up times J^*, emerging from the direct, open-loop optimization. In Table III the results of the benchmark analysis are shown. For the situations investigated, the maximum relative performance loss of the controller with respect to the open-loop optimized solution δJ, is 2.3%. This result not only indicates that the assumptions and approximations made are feasible in principle, but it legitimates the methods applied for the controller development and implementation.

F. Investigation of Alternative System Configurations

After the detailed analysis of the control law, the proposed configuration of the power system (fuel cell system with electrical heater and battery), was compared with alternative system configurations in terms of the duration of the warm-up phase. To this end, three alternative configurations were proposed first:

#1: fuel cell power system without battery nor heater;
#2: fuel cell/battery hybrid power system without heater;
#3: fuel cell power system without battery but with an electrical auxiliary heater.

The system configuration proposed in this text (battery and heater) is termed as configuration #0. In a second step direct, open-loop optimizations (based on the detailed model equations) were performed to compute the optimal performance values of the four configurations, under the nominal operating conditions of case 2 (Table II). Charge-sustaining operation

TABLE IV
OPTIMAL PERFORMANCES OF DIFFERENT SYSTEM CONFIGURATIONS UNDER NOMINAL OPERATING CONDITIONS (CASE 2 OF TABLE II)

#	Battery/Heater	I_{St}^{Des}	u_{Ht}	J^* (s)	$\delta J^{*\dagger}$ (%)
#1	No/No	$f(P_{Out})$	-	4250	-
#2	Yes/No	opt.	-	943	-77.8
#3	No/Yes	$f(P_{Out}, u_{Ht})$	opt.	425	-90.0
#0	Yes/Yes	opt.	opt.	309	-92.7

† Relative performance difference with respect to configuration #1: $\delta J^* = (J^* - J^*|_{\#1})/J^*|_{\#1}$

was enforced for configurations containing a battery. The computed performance values J^*, i.e., the minimal warm-up times, are shown in Table IV. The configuration without battery nor heater (configuration #1) serves as a basis for the comparison. Under nominal operating conditions this system takes almost 1.2 h (4250 s) to reach the operating temperature of 50 °C. The hybridization with a battery reduces the elapsed warm-up time by 78% to 943 s, provided that an optimal power management is applied. Another 67% reduction to 309 s can be gained by adding an (optimally operated) auxiliary heater. Hence, the combination of hybridization and auxiliary heating yields a warm-up time of 7% of the reference value of configuration #1. A system configuration with auxiliary heater but without battery (configuration #3) has a warm-up period reduced by 90%, with respect to the warm-up time of the reference configuration.

The improvement achieved with the hybridization is explained by the additional degree of freedom.[16] As a direct consequence of the possibility to store energy, the fuel cell stack can be operated independently of the power demand, hence, only part time and at a higher (maximum) current. This, in turn, results in an increased production of heat and reduced losses of heat to the ambient. Similarly, the auxiliary heater adds a degree of freedom to the system as well, but the heater has two effects on the warm-up behavior. Primarily, it delivers energy to the system directly in terms of heat. Secondarily, and analogously to the battery, it permits the fuel cell stack to be operated on a higher power level. However, in contrast to the battery, the heater does not allow the fuel cells to be operated completely decoupled from the power demand.

VII. CONCLUSIONS

With the optimal supervisory power controller developed in this project, an important contribution is made to mitigating the problems concomitant with the warm-up phase of a hybrid fuel cell power system. The controller operates a fuel cell/battery hybrid power system that is equipped with an auxiliary heater during the transient phase after a cold start, ensures a fast, charge-sustaining system warm-up, and considers the temperature-induced power limitations of the fuel cells. It is model-based and implemented as a feedback controller.

The aim of minimizing the duration of the system warm-up was formulated as an optimal control problem. From the necessary conditions of Pontryagin's minimum principle, a solution to the problem was educed. In particular, the appropriate combination of the conditions for optimality and the careful statement of simplifications and assumptions allowed the formulation of the solution as a feedback control law. Due to its simple structure, this control law is suited to be applied online. In order to determine the control signals, no numerical optimization is required but only the solution of one implicit equation has to be computed, aside from algebraic calculations. Moreover, the application of the control law to different systems should be feasible with minor efforts only, since its design is model-based.

A simulated system warm-up demonstrated the functionality of the controller. The performance of the controller was verified with a direct, open-loop optimization for various operating conditions and controller settings. The results confirmed the functions of the control system derived as the relative performance losses, which mainly originate from the simplifications made during the controller design, amount to a few percent only. Finally, an analysis of various system configurations proved the benefits of a hybrid setup including an auxiliary heater in terms of a fast system warm-up. For the optimally controlled configuration proposed, the simulation showed a drastically reduced warm-up time, compared with the warm-up duration of a pure fuel cell system without battery nor auxiliary heater.

APPENDIX I
REDUCED-ORDER MODEL

In the following, the equations of the reduced-order model are given. The state variables are the mean system temperature T_{FCS} and the battery state of charge SoC. Unless otherwise stated, the parameters of the model are assumed to be constant.

The temperature characteristics of the system are captured by the following differential equation:

$$\frac{d}{dt}T_{FCS} = \frac{1}{(mC)_{FCS}}\Big[\left(V_{St}^0 - V_{St}\right) I_{St}^{Des} - \dot{H}_{H_2O}^{Evap} - \dot{Q}_{Conv}^{FCS2Amb} - \dot{Q}_{Rad}^{FCS2Amb} + \dot{Q}_{Ht2FCS}\Big]. \quad (55)$$

The parameter V_{St}^0 is the reversible open circuit voltage of the stack for standard conditions

$$V_{St}^0 = n_{Cells}\frac{(h_f^0)_{H_2O(l)} M_{H_2O}}{2F}. \quad (56)$$

The stack voltage is calculated as

$$V_{St} = n_{Cells} V_{Cell}(i_{St}, T_{FCS}, p_{O_2}^{Ca}, p_{H_2}^{An}) \quad (57)$$

where the cell voltage V_{Cell} follows from the voltage model presented in [9]. The cell voltage is a function of the current density i_{St}, of the system temperature T_{FCS}, and of the partial pressures of the oxygen in the cathode and of the hydrogen in the anode $p_{O_2}^{Ca}$ and $p_{H_2}^{An}$, respectively. The equations to calculate these quantities from the input signals are given as follows. The current density generated at the membrane surface area A_{Active} is defined as

$$i_{St} = \frac{I_{St}^{Des}}{A_{Active}}. \quad (58)$$

The partial pressure of oxygen in the cathode is calculated from

$$p_{O_2}^{Ca} = y_{O_2}^{Ca}\left(p_{Ca} - \varphi_{Ca} p_{Sat\ H_2O}(T_{FCS})\right) \quad (59)$$

[16]Note that for configurations without an energy storage unit (configurations #1 and #3), the stack current follows directly from the total power demand.

where the mean oxygen mole fraction of air in the cathode $y_{O_2}^{Ca}$, the mean cathode relative humidity φ_{Ca}, and the mean cathode pressure p_{Ca}, follow as

$$y_{O_2}^{Ca} = \frac{2\lambda_{Air}^{Des} - 1}{2\lambda_{Air}^{Des} - y_{O_2}^{Air}} y_{O_2}^{Air} \tag{60}$$

$$\varphi_{Ca} = \frac{1}{2}\left(\varphi_{mAir}^{HS\,Out} + \varphi_{mAir}^{PS\,Out}\right) \tag{61}$$

$$p_{Ca} = \frac{1}{2}\left(p_{mAir}^{HS\,Out} + p_{Amb}\right). \tag{62}$$

For the estimation of the pressure at the cathode inlet (the humidifier outlet), a linear nozzle equation (with nozzle constant γ_{Ca}) is proposed

$$p_{mAir}^{HS\,Out} = p_{Amb} + \frac{\dot{m}_{Air}^{HS\,In}}{\gamma_{Ca}} \tag{63}$$

where the mass flow rate of air is proportional to the electric current

$$\dot{m}_{Air}^{HS\,In} = \lambda_{Air}^{Des} \frac{M_{Air} n_{Cells}}{4F y_{O_2}^{Air}} I_{St}^{Des}. \tag{64}$$

The partial pressure of hydrogen in the anode follows as

$$p_{H_2}^{An} = p_{An} - \varphi_{An} p_{Sat\,H_2O}(T_{FCS}). \tag{65}$$

The term $\dot{H}_{H_2O}^{Evap}$ in (55) represents the enthalpy flow rate due to evaporation. It results from a water mass balance between air inlet and air outlet

$$\dot{H}_{H_2O}^{Evap} = \left\{ \left[I_{St}^{Des} \frac{n_{Cells} M_{O_2}}{4F} \left(\lambda_{Air}^{Des} \frac{1}{y_{O_2}^{Air}} \frac{M_{Air}}{M_{O_2}} - 1 \right) \cdot \frac{\varphi_{mAir}^{PS\,Out} p_{Sat\,H_2O}(T_{FCS})}{p_{Amb} - \varphi_{mAir}^{PS\,Out} p_{Sat\,H_2O}(T_{FCS})} \right] \cdot \frac{M_{H_2O}}{M_{Air}} - \dot{m}_{H_2O}^{mAir HS\,In} \right\} h_{fg\,H_2O}(T_{FCS}). \tag{66}$$

The remaining terms in (55) consider the convective and the radiative heat losses to the ambient and the heat flow rate supplied by the coolant heater

$$\dot{Q}_{Conv}^{FCS2Amb} = \alpha_{FCS2Amb} A_{FCS2Amb} (T_{FCS} - T_{Amb}) \tag{67}$$

$$\dot{Q}_{Rad}^{FCS2Amb} = \sigma \varepsilon_{FCS2Amb} A_{FCS2Amb} \left(T_{FCS}^4 - T_{Amb}^4\right) \tag{68}$$

$$\dot{Q}_{Ht2FCS} = \dot{Q}_{Ht}^{Nom} u_{Ht}. \tag{69}$$

Note that the impact of the cooling system fan could easily be included in the model. The battery state of charge is given by the following relation:

$$\frac{d}{dt}\mathrm{SoC} = \begin{cases} -\frac{1}{Q_{Bat}} I_{Bat}, & \text{if } I_{Bat} \geq 0 \\ -\frac{1}{Q_{Bat}} \eta_{Bat} I_{Bat}, & \text{if } I_{Bat} < 0 \end{cases} \tag{70}$$

where the battery current I_{Bat}, is calculated as

$$I_{Bat} = \frac{V_{OC}^{Av} - \sqrt{\left(V_{OC}^{Av}\right)^2 - 4R_i^{Av} P_{Bat}}}{2R_i^{Av}}. \tag{71}$$

```
1) u1 = 0
2) if γ < 0
     u2 = 1
   else
     u2 = 0
   end
3) if β + δ · u2 < 0
     ū1 = 1
   else
     ū1 = 0
   end
4) if ū1 ≠ u1
     u1 = 1
     if γ − δ < 0
       u2 = 1
     else
       u2 = 0
     end
   end
```

Fig. 8. Possible algorithm to determine the controls u_1^* and u_2^*.

The battery current is a function of the battery power P_{Bat}, which follows from the following equation:

$$P_{Bat} = P_{Out} + \frac{\dot{Q}_{Ht}^{Nom}}{\eta_{Ht}} u_{Ht} - \eta_{PC} V_{St}(I_{St}^{Des}, T_{FCS}, \lambda_{Air}^{Des}, p_{Amb}) I_{St}^{Des}. \tag{72}$$

Appendix II
Resolving the Implicit Relations of the Preliminary Control Laws

In this appendix an approach is shown which serves to uniquely determine the controls u_1^* and u_2^* from the implicit relations (44a)–(c). The cases where the switching functions vanish are not relevant, as the switching functions can only vanish at isolated instants of time. If these cases are excluded, the preliminary control laws (44a)–(c) can be restated as

$$u_1^* = \begin{cases} 1, & \text{if } \beta(x_1^*, \lambda_2^*, v) + \delta(x_1^*, \lambda_2^*, v) u_2^* < 0 \\ 0, & \text{if } \beta(x_1^*, \lambda_2^*, v) + \delta(x_1^*, \lambda_2^*, v) u_2^* \geq 0 \end{cases} \tag{73a}$$

and

$$u_2^* = \begin{cases} 1, & \text{if } \gamma(x_1^*, \lambda_2^*, v) - \delta(x_1^*, \lambda_2^*, v) u_1^* < 0 \\ 0, & \text{if } \gamma(x_1^*, \lambda_2^*, v) - \delta(x_1^*, \lambda_2^*, v) u_1^* \geq 0 \end{cases} \tag{73b}$$

respectively. As the linear terms of the switching functions in (73a) and (b) have different signs, the controls u_1^* and u_2^* are uniquely determined by the control laws (73a) and (b). A possible algorithm to determine the controls u_1^* and u_2^*, given the coefficients $\beta(x_1^*, \lambda_2^*, v)$, $\gamma(x_1^*, \lambda_2^*, v)$, and $\delta(x_1^*, \lambda_2^*, v)$, is shown in Fig. 8.

Acknowledgment

The authors would like to acknowledge the support of D. McKay from the Fuel Cell Control Systems Laboratory, University of Michigan.

References

[1] M.-J. Kim and H. Peng, "Combined control/plant optimization of fuel cell hybrid vehicles," in *Proc. Amer. Contr. Conf.*, 2006, pp. 496–501.

[2] K. S. Jeong, W. Y. Lee, and C. S. Kim, "Energy management strategies of a fuel cell/battery hybrid system using fuzzy logics," *J. Power Sources*, vol. 145, no. 2, pp. 319–326, Aug. 2005.

[3] I. Arsie, C. Pianese, A. Di Domenico, and M. Sorrentino, "Transient analysis of PEM fuel cell for hybrid vehicle application," presented at the 3rd Int. Conf. Fuel Cell Sci., Eng. Technol., Ypsilanti, MI, 2005.
[4] P. Rodatz, G. Paganelli, A. Sciarretta, and L. Guzzella, "Optimal power management of an experimental fuel cell/supercapacitor-powered hybrid vehicle," *Contr. Eng. Practice*, vol. 13, no. 1, pp. 41–53, Jan. 2005.
[5] Z. H. Jiang, L. J. Gao, M. J. Blackwelder, and R. A. Dougal, "Design and experimental tests of control strategies for active hybrid fuel cell/battery power sources," *J. Power Sources*, vol. 130, no. 1–2, pp. 163–171, May 2004.
[6] M. J. Gielniak and Z. J. Shen, "Power management strategy based on game theory for fuel cell hybrid electric vehicles," in *Proc. IEEE Veh. Technol. Conf.*, 2004, pp. 4422–4426.
[7] E. A. Müller and A. G. Stefanopoulou, "Analysis, modeling, and validation for the thermal dynamics of a polymer electrolyte membrane fuel cell system," *J. Fuel Cell Sci. Technol.*, vol. 3, no. 2, pp. 99–110, May 2006.
[8] L. Guzzella, "Control oriented modeling of fuel-cell based vehicles," presented at the NSF Workshop Integr. Modeling Contr. Autom. Syst., Santa Barbara, CA, 1999.
[9] A. L. Schilter, D. A. McKay, and A. G. Stefanopoulou, "Parameterization of fuel cell stack voltage: issues on sensitivity, cell-to-cell variation, and transient response," presented at the 4th Int. Conf. Fuel Cell Sci., Eng. Technol., Irvine, CA, 2006.
[10] D. D. Boettner, G. Paganelli, Y. G. Guezennec, G. Rizzoni, and M. J. Moran, "Proton exchange membrane fuel cell system model for automotive vehicle simulation and control," *J. Energy Resources Technol.*, vol. 124, no. 1, pp. 20–27, Mar. 2002.
[11] V. H. Johnson, "Battery performance models in ADVISOR," *J. Power Sources*, vol. 110, no. 2, pp. 321–329, Aug. 2002.
[12] L. Guzzella and A. Sciarretta, *Vehicle Propulsion Systems: Introduction to Modeling and Optimization*. Berlin, Germany: Springer-Verlag, 2005.
[13] C.-W. Park and A. K. Jaura, "Reciprocating battery cooling for hybrid and fuel cell vehicles," in *Proc. Int. Mechan. Eng. Congress*, 2003, pp. 425–430.
[14] ——, "Transient heat transfer of 42 V Ni-MH batteries for an HEV application," presented at the Future Car Congress, Arlington, VA, 2002.
[15] M. Athans and P. L. Falb, *Optimal Control: An Introduction to the Theory and Its Applications*. New York: McGraw-Hill, 1966.
[16] H. P. Geering, H. Domeisen, F. Weinberg, K. Hazeghi, A. Polyméris, H.-J. Lüthi, H. G. Benninger, and F. Benito, *Optimierungsverfahren zur Lösung deterministischer regelungstechnischer Probleme*. Bern; Stuttgart: Haupt, 1982.
[17] O. Barbarisi, F. Vasca, and L. Glielmo, "State of charge Kalman filter estimator for automotive batteries," *Contr. Eng. Practice*, vol. 14, no. 3, pp. 267–275, Mar. 2006.
[18] J. Chiasson and B. Vairamohan, "Estimating the state of charge of a battery," *IEEE Trans. Contr. Syst. Technol.*, vol. 13, no. 3, pp. 465–470, May 2005.
[19] D. A. McKay, W. T. Ott, and A. G. Stefanopoulou, "Modeling, parameter identification, and validation of reactant and water dynamics for a fuel cell stack," presented at the Int. Mechan. Eng. Congress Exposition, Orlando, FL, 2005.
[20] D. A. McKay and A. G. Stefanopoulou, "Parameterization and validation of a lumped parameter diffusion model for fuel cell stack membrane humidity estimation," in *Proc. Amer. Contr. Conf.*, 2004, pp. 816–821.
[21] *"GESOP Software User Manual, GESOP SUM 4.6.0,"* Inst. Flight Mechan. Contr., Univ. Stuttgart, Stuttgart, Germany, Feb. 2004.

Eric A. Müller was born in Uster, Switzerland, in 1977. He received the Diploma (Master's equivalent) in mechanical engineering in 2002 from ETH Zurich, Zurich, Switzerland.

Since 2002, he has been working as a doctoral student and a research/teaching assistant at the Measurement and Control Laboratory at ETH Zurich. His research interests include modeling and optimal control of thermal systems, especially for automotive applications.

Anna G. Stefanopoulou (SM'05) received the Diploma from the National Technological University of Athens, Greece, in 1991, the M.S. degree in naval architecture and marine engineering, a second M.S. degree in electrical engineering and computer science, and the Ph.D. degree from the University of Michigan, Ann Arbor, in 1992, 1994, and 1996, respectively.

Currently, she is a Professor in the Mechanical Engineering Department at the University of Michigan. She was an Assistant Professor (1998–2000) at the University of California, Santa Barbara, and a Technical Specialist (1996–1997) at the Scientific Research Laboratories at Ford Motor Company, Dearborn, MI. Her current research interests include control of advanced internal combustion engines and fuel cell power systems.

Lino Guzzella (SM'05) was born in Zurich, Switzerland, in 1957. He received the Diploma in mechanical engineering and the Dr. sc. techn. degree in control engineering from ETH Zurich, Zurich, Switzerland, in 1981 and 1986, respectively.

He is currently a Professor for thermotronics in the Mechanical Engineering Department of ETH Zurich. From 1987 to 1989, he was with the Research and Development Department of Sulzer Brothers, Winterthur, Switzerland. From 1989 to 1991 he was an Assistant Professor for automatic control in the Electrical Engineering Department of ETH Zurich. He then joined Hilti Research and Development, Schaan, Liechtenstein, where he was the head of the Mechatronics Department from 1992 to 1993. His research interests include modeling and optimization of dynamic systems, nonlinear and robust control, and applications of these ideas to thermal and especially automotive systems.